Vascular Complexity Evaluation Using a Skeletonization Approach and 3D LED-Based Photoacoustic Images

Kristen M. Meiburger, Alberto Vallan, Silvia Seoni, and Filippo Molinari

Abstract Vasculature analysis is a fundamental aspect in the diagnosis, treatment, outcome evaluation and follow-up of several diseases. The quantitative characterization of the vascular network can be a powerful means for earlier pathologies revealing and for their monitoring. For this reason, non-invasive and quantitative methods for the evaluation of blood vessels complexity is a very important issue. Many imaging techniques can be used for visualizing blood vessels, but many modalities are limited by high costs, the need of exogenous contrast agents, the use of ionizing radiation, a very limited acquisition depth, and/or long acquisition times. Photoacoustic imaging has recently been the focus of much research and is now emerging in clinical applications. This imaging modality combines the qualities of good contrast and the spectral specificity of optical imaging and the high penetration depth and the spatial resolution of acoustic imaging. The optical absorption properties of blood also make it an endogenous contrast agent, allowing a completely non-invasive visualization of blood vessels. Moreover, more recent LED-based photoacoustic imaging systems are more affordable, safe and portable when compared to a laser-based systems. In this chapter we will confront the issue of vessel extraction techniques and how quantitative vascular parameters can be computed on 3D LED-based photoacoustic images using an in vitro vessel phantom model.

K. M. Meiburger (✉) · A. Vallan · S. Seoni · F. Molinari
PoliToBIOMed Lab, Department of Electronics and Telecommunications, Politecnico di Torino, Turin, Italy
e-mail: kristen.meiburger@polito.it

A. Vallan
e-mail: alberto.vallan@polito.it

S. Seoni
e-mail: silvia.seoni@polito.it

F. Molinari
e-mail: filippo.molinari@polito.it

M. Kuniyil Ajith Singh (ed.), *LED-Based Photoacoustic Imaging*,
Progress in Optical Science and Photonics 7,
https://doi.org/10.1007/978-981-15-3984-8_5

1 Introduction

Blood vessels play a fundamental role in the well-being of tissues, organs and organ systems, by providing them with oxygen and nutrients and subsequently eliminating waste products. Many diseases affect blood vessels and their attributes, such as their number, size, or pattern [1]. For example, tumors typically induce the growth of many vessel clusters with an abnormal tortuosity and smaller diameter, while chronic inflammations induce neoangiogenesis [1, 2]. It is therefore evident how the possibility of a non-invasive and quantitative evaluation of 3D vessel attributes is essential for early diagnosis and the staging of various diseases [1].

Many imaging techniques can be used for visualizing vasculature structures. For example, computed tomographic angiography (CTA) has an excellent spatial resolution and it is very common in clinics. As a downside, however, it uses ionizing radiations and iodinated contrast agents. Magnetic resonance angiography (MRA) in spite of very good contrast and temporal resolutions and lack of ionizing radiation, suffers from rapid extravasation of the contrast agent that affects the accuracy, and is a very expensive imaging modality. Doppler ultrasound imaging (DU) has much lower costs, large availability and it doesn't use nephrotoxic contrast agents, but it is operator-dependent, contrast agents typically have short duration and this imaging technique is typically sensitive only to larger vessels and is not able to highlight microvasculature. Also, a more recent technique, acoustic angiography, that uses dual-frequencies ultrasound transducers for the minimization of background [3] needs exogenous contrast agents and custom-made probes, while optical coherence tomography angiography (OCTA) has a limited penetration depth and a longer acquisition time [4, 5].

Photoacoustic imaging is an imaging modality that has seen an exponential growth over the last couple of decades. Using this technique, ultrasound signals are generated from the interaction between a pulsed light source at a given wavelength and the biological tissues that are irradiated. So, it is non-invasive and non-ionizing and it combines the high spatial resolution and the penetration depth of ultrasound with the high contrast and the spectral specificity of optical imaging [6, 7]. In particular, the visualization of blood vessels is a main application of photoacoustic imaging, as oxygenated and deoxygenated haemoglobin give forth a strong photoacoustic signal at various wavelengths and therefore present an endogenous contrast agent for this imaging modality [8, 9].

Typically, laser light sources are used for photoacoustic imaging, but these optical systems are typically cumbersome, expensive, and they usually have fluctuations of wavelength and power per pulse. Moreover, safety glasses or a shield is necessary to protect the operator and/or patient from the irradiation of the light source. Much recent research has focused on the use of different light sources, and in particular on the use of pulse laser diodes. In fact, light emitting diodes (LEDs) are inexpensive, compact, multi-wavelength and more stable. LED-based systems are therefore more portable and an enclosure or protective glasses aren't necessary [7]. However, due

to the reduced energy the LED light source is able to emit compared to laser light sources, these systems typically are limited to more superficial imaging applications.

In this chapter, we will present a proof of concept and feasibility study of using 3D LED-based photoacoustic images for the quantitative evaluation of the vascular complexity network using a skeletonization approach and an in vitro phantom model. First of all, the numerous techniques for vessel extraction from images are presented and summarized. Then, quantitative vascular parameters that are used to describe vascular networks and that have been used in numerous studies are defined and explained. Finally, we then present our approach for the phantom model definition, image acquisition and processing steps, and validation results.

2 Blood Vessel Extraction Techniques

Many various methods have been introduced to automatically extract the vascular network from medical images. The main differences between techniques are due to pre-processing steps, computational time, accuracy, and the visual quality of the obtained results [10].

Four main categories of blood vessel extraction techniques can be defined: pattern recognition approaches, model-based approaches, vessel tracking approaches, and machine learning approaches. It is also possible to combine the use of different techniques together to improve the final results [11]. In this section, we will briefly explore the four main categories of blood vessel extraction methods and the numerous methods that are included in each main category.

2.1 Pattern Recognition Techniques

Pattern recognition techniques are methods that are used for the automatic detection and classification of various objects. In the specific application of vessel extraction, they detect vessel-like structures and features, and there are many different approaches that can be classified within this main category, such as multi-scale, skeleton-based, and ridge-based [12].

2.1.1 Multi-scale

Multi-scale approaches are based on extracting the vasculature at different levels of resolution. The vessels with a larger diameter are extracted using images with a lower resolution, since less detail is needed to correctly extract the vessel, whereas the smaller vessels and microvasculature are extracted using images with a higher resolution [12]. Instead of using images with an actual different resolution, multi-scale methods found in literature can also be based on using kernels with different

scales that enhance vessels with diameters of a certain dimension, such as the well-known and applied Frangi filter [13].

2.1.2 Skeleton-Based

Skeleton-based vessel extraction techniques are employed to extract the blood vessel centerlines and the entire vessel structure is created by connecting the vessel centerlines. These kinds of techniques are based on first segmenting the vessels using various approaches (such as thresholding), and the segmentation is then thinned using a specific algorithm, such as the medial axis thinning algorithm [14]. The skeletonization process is used to reduce the segmentation to a minimal representation that keeps the morphology without redundancy.

Figure 1 shows some examples of skeletons obtained using various imaging modalities.

2.1.3 Ridge-Based

Ridge-based vessel extraction techniques are based on the idea that grayscale image can be seen as a 3D elevation map where intensity ridges approximate the skeleton of objects that adopt a tubular shape [12]. In this way, ridge points are simply local peaks in the direction of the maximal surface gradient and are invariant to affine transformations.

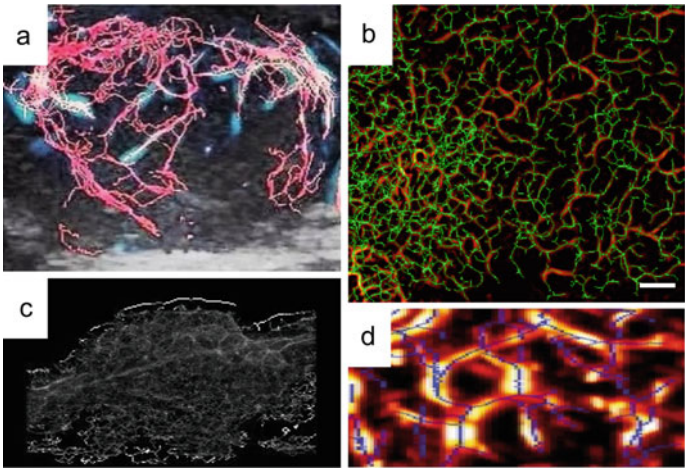

Fig. 1 Examples of skeletons obtained with different imaging modalities. **a** Doppler ultrasound imaging, skeleton in red. **b** Optical coherence tomography angiography, skeleton in green. **c** Contrast-enhance ultrasound imaging. **d** Photoacoustic imaging, skeleton in blue

2.1.4 Region Growing

Region growing approaches are those based on segmenting the vessel network through a region growing technique that segments images by analyzing neighboring pixels and assigning them to specific objects based on their pixel value similarity and spatial proximity [12]. A downfall to this kind of approach is that it is necessary to provide some form of seed point from which to start the region growing analysis, and these typically must be supplied by the user.

2.1.5 Differential Geometry-Based

Differential geometry-based vessel extraction methods consider the acquired images as hypersurfaces and therefore extracts features, thanks to the crest lines and curvature of the surface. The center lines of the vessels are therefore found as the crest points of the hypersurface. In this way, a 3D surface can be described by two principal curvatures (i.e., the eigen values of the Weingarten matrix) and their principal directions (i.e., the eigenvectors), which are their corresponding orthogonal directions [12].

2.1.6 Matching Filters

Vessel extraction techniques based on matching filters are used to find objects of interest by convolving the image with multiple matched filters. The design of different filters in order to detect vessels with different orientation and size plays a fundamental role with this type of approach, and the convolutional kernel size directly affects the computational load of the method.

2.1.7 Mathematical Morphology

Methods based on mathematical morphology schemes rely on the use of morphological operators to enhance vessel structures from the image. Morphological operators are defined by applying specific structuring elements to the image, which define the operator locality and can take on various geometries, such as a line, circle, square, diamond, etc. The two main morphological operators are dilation and erosion, which expands or shrinks objects, respectively. These operators can therefore be exploited to enhance vessel structures and/or remove areas of the image that are not vessels.

2.2 Model-Based Techniques

As their name implies, model-based techniques for vessel extraction apply explicit models to extract the vasculature from the images. These methods can be divided into four main different categories, which are briefly explored more in detail below.

2.2.1 Parametric Deformable Models

Parametric deformable models, often also known as snakes, are techniques that aim to find object contours using parametric curves that deform under the influence of internal and external forces. Internal forces are important for the smoothness of the surface, while external ones attract it to the vessel boundary. The smoothness constraint is the elasticity energy and makes the model more robust to the noise. A downside of these models is that in order to start the process, the surface has to be initialised and the model evolution depends on initial parameters that must be fine-tuned by the user. Moreover, it is fundamental that the final model is robust to its initialization. With recent implementations, it's also possible to insert constraints or a priori knowledge about geometry [12, 15]. These approaches are suitable for complex architecture or variable vessels, but they are very time consuming.

2.2.2 Geometric Deformable Models

Geometric deformable models are based on the theory of curve evolution, and are commonly known as level sets [12]. Level sets are based on the main concept that propagating curves are represented as the zero-level set of a higher dimensional function, which is typically given in the Eulerian coordinate system. This type of approach has the following advantages: (1) it can handle complex interfaces that present sharp corners and change its topology during the level set evolution; (2) the curvature and normal to the curve, which are intrinsic properties of the propagating front, can be easily extracted from the level set function; (3) it is easily extendable to problems of higher dimensions, and is therefore not limited to 2D images.

2.2.3 Parametric Models

Parametric models (PM), not to be confused with parametric deformable models, define parametrically the object of interest. In particular, for tubular objects, they are described as a set of overlapping ellipsoids. In some applications, the model of the vessel is circular. The estimation of parameters is done from the image, but the elliptic PM approximates healthy vessels well but not pathological shapes and bifurcations [12].

2.2.4 Template Matching

This method attempts to recognize a structure, an a priori model or template, in the image. This is a contextual top-down method. For the application of arterial extraction, the template is a set of nodes connected in segments, that then is deformed to fit the real structure. For the deformation, a stochastic process can be used [12].

2.3 Vessel Tracking Techniques

Vessel tracking approaches apply local operators on a focus known to be a vessel and track it. They differ from pattern recognition approaches in that they do not apply local operators to the entire image. So, starting from an initial point, these methods detect vessel centerlines or boundaries by analyzing the pixels orthogonal to the tracking direction [12].

2.4 Machine Learning

Machine learning is a subfield of artificial intelligence in which computers learn how to solve a specific problem from experimental data.

These approaches can be divided in unsupervised and supervised:

- Unsupervised approaches try to find a model that describes input images no having prior knowledge about them. This technique doesn't need the comparison with a gold standard.
- Supervised approaches learn the model from a training set of labelled images and then applies it to the input images. This technique has shown better performances, and testing the trained network is typically very fast. On the other hand, training the network typically requires a huge computational cost [11].

Recently, there has been a huge growth of the application of supervised machine learning approaches under the form of neural networks and specifically convolutional neural networks (CNNs) in the application of image processing. CNNs are characterized by the presence of convolutional layers for feature extraction, pooling layers for feature reduction and fully connected layers for classification [11].

3 Vessel Architecture Quantification

As discussed in the previous section, there are numerous methods that can be exploited to extract the vessel network from images acquired using various imaging modalities. All of these methods aim to extract the vessel network from the images, so

that the vessels can further be classified and/or analyzed to gain important information about the tissue or organ health status.

Many studies in literature are based on qualitative or semi-quantitative analyses of the extracted vessel network, by either visually observing the enhanced or segmented network or by manually selecting specific vessels to analyze with more quantitative methods [1, 3, 16, 17].

In this chapter, and specifically in this section, we will go more into details about how a quantitative analysis of the vessel network can be obtained and what quantitative parameters can be computed from the skeleton of the vessel network.

As described previously, the skeleton of a vessel is a minimal representation of the segmented vessels, which can be independent of the imaging modality used to acquire the images. In fact, the main goal is to segment the vessels from the images and once the segmentation is obtained using the desired technique, the skeleton of the vessels can be obtained by applying, for example, the medial axis thinning algorithm [14]. Many techniques based on skeletonization have been used in literature to extract the vessel network and then used to calculate quantitative parameters that can help distinguish healthy from diseased tissue in numerous imaging modalities, such as in CT images of the lung [18], ultrasound contrast-enhanced clinical images of the thyroid to characterize thyroid nodules [19, 20], ultrasound contrast-enhanced images of tumors in murine models [21], photoacoustic images of burn wounds in rats to differentiate from healthy tissue [4], and optical coherence tomography angiography (OCTA) images of clinical dermatological lesions for the automatic segmentation of the lesion [22].

An important step before quantitative parameter calculation is the placement of a specific region-of-interest (ROI) within which to calculate the parameters. This is to help reduce the computational load, and is due to the fact that typically vasculature is present not only in the area that is of interest (for example, outside of the tumor or diseased tissue), and more importantly, due to the fact that these quantitative parameters should not be considered using their absolute values, but in comparison with the same parameters either at a different location or at a different time. So, the relative comparison between the parameters gives a better evaluation rather than the actual value by itself.

In all of the studies mentioned previously, the ROI is manually placed on the desired areas, except for in the most recent study by Meiburger et al. [22] in which the entire OCTA volume was analyzed by a sliding ROI. The quantitative vascular parameters computed inside each ROI were then employed to automatically define the lesion area. Subsequently, the ROI for the diseased zone was automatically placed in correspondence of the centroid of the defined lesion area and the healthy zone was automatically placed in correspondence of the ROI that was found to be furthest away from the considered diseased ROI.

In the next section we will go into more detail about what specific quantitative parameters can be computed on the skeleton of the vessel network within the defined ROI, which can be classified as either morphological or tortuosity parameters.

3.1 Morphological Parameters

As the name implies, morphological parameters give an idea of the morphology of the considered vessel network, taking into consideration their size, how many vessels are present, and how they are distributed between each other. The principal quantitative morphological parameters that have been used in previous studies are:

- Number of trees (NT): defined as the number of vessel trees in which the skeleton is decomposed
- Vascular density (VD): defined as the ratio between the number of skeleton voxels and the total number of voxels of the considered ROI
- Number of branching nodes (NB): defines as the number of branching nodes that are found in the vessel structure
- Mean radius (MR): mean radius of the segmented vessels of the structure.

While the first three parameters are consistently used in various studies, the mean radius is a quantitative parameter that is sometimes excluded, due to the fact that it the one that is most highly dependent on an accurate segmentation of the actual borders of the vessels. Thanks to the skeletonization process, a slightly oversegmented or undersegmented vessels do not influence the first three quantitative parameters (i.e., NT, VD, and NB). On the other hand, the mean radius is highly influenced by an inaccurate segmentation, which is the reason why this parameter is sometimes omitted in various studies.

3.2 Tortuosity Parameters

Tortuosity parameters are those parameters that analyze the path of the vessels and how curved, tortuous or tightly coiled the vessel path may be. In order to calculate these parameters, it is fundamental to first "isolate" a specific vessel to analyze and then begin from one end point and arriving at the other end point, various quantitative parameters can be calculated along the path, either by measuring angles, inflection points, or simply path length.

Specifically, three main quantitative tortuosity parameters are typically calculated to give an idea of the tortuosity of the considered vascular network:

- 2D distance metric (DM): defined as the ratio between the actual path length of the considered vessel and the linear distance between the first and last endpoint of the vessel
- Inflection count metric (ICM): defined as the 2D distance metric multiplied by the number of inflection points found along the vessel path
- 3D sum of angles metric (SOAM): defined as the sum of all the angles that the vessel has in space.

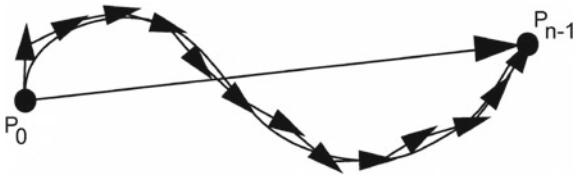

Fig. 2 Graphical representation of 2D distance metric computation

The mathematical descriptions of these tortuosity parameters can be found in previously published studies [1, 23].

Briefly, the DM gives a measure of the bidimensional tortuosity of the considered vessel, since a straight line would give forth a value of 1, and as the vessel potentially becomes more and more curved, the DM value will increase. Figure 2 shows a graphical representation of how the DM is computed. The ICM adds to the DM as it considers not only the overall curvature of the considered vessel, but also the number of times the vessel changes direction in its path. Finally, the SOAM parameters are helpful mostly in the case of tightly coiled vessels, which are not well-represented by either the DM or ICM.

4 Phantom Design

In this section of the chapter, we will describe how a possible vascular phantom can be designed to show the feasibility of evaluation the vascular complexity using a skeletonization approach and 3D LED-based photoacoustic images.

In medical imaging, phantoms are samples with known geometry and composition that mimic biological tissues with their physical and chemical properties for providing a realistic environment for clinical imaging applications. Stable and well characterized phantoms are very useful for routine quality controls, training, calibration and for evaluating the performance of systems and algorithms. They can be also used for the development of new applications before in vivo preclinical or clinical studies. Moreover, phantoms allow to understand reproducibility in time and among laboratories, to optimize signal to noise ratio, to compare detection limits and accuracies of different systems and to examine maximum possible depth [24–27].

4.1 Model Design

In order to correctly evaluate vascular complexity, it is first necessary to design a model that can represent in a simplified manner at least a section of a vascular network. An example of a method that can be used to mimic a vascular network is the creation of a 3D model which can then be printed using various materials.

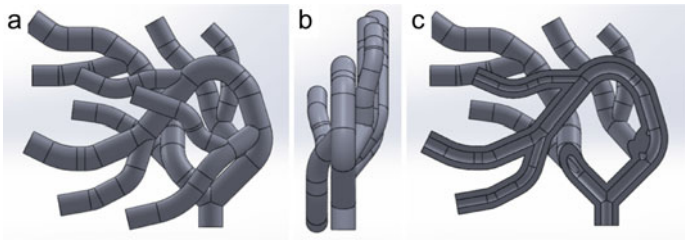

Fig. 3 3D model designed for vascular complexity analysis. **a** Front view. **b** Lateral view. **c** Section view

As a proof of concept, we designed a model using a computer aided design software that had the following dimensions: 39.23 mm × 34.37 mm × 12.78 mm with a wall thickness of 1 mm. The internal diameter of the designed vessels was equal to 1.5 mm. Figure 3 shows the designed model from a front view (a), lateral view (b) and section view (c).

4.1.1 3D Printing

Once the model was designed, we then proceeded to use a 3D printer to print the model. In this preliminary proof of concept study, we used the ProJet MJP 2500 Plus with the VisiJet R Armor (M2G-CL) material, a tough, ABS-like clear plastic that combines tensile strength and flexibility [28].

The ProJet MJP 2500 Plus is a 3D MultiJet printer that uses the inkjet printing process. In particular, a piezo printhead deposits a plastic resin and a casting wax material through the layer by layer technique.

Then the MJP EasyClean System is used to remove in a little time, the support material from plastic parts using steam and EZ Rinse-C. It is composed of two warmer units, one for bulk wax removal and one for fine wax removal. The support material is separated by melting or dissolving. This is a non-contact method, so there are less substrates or mask damages and contamination. Moreover, it permits a high resolution and is inexpensive. Figure 4a shows an image acquired during the 3D printing process and the final obtained model (Fig. 4b).

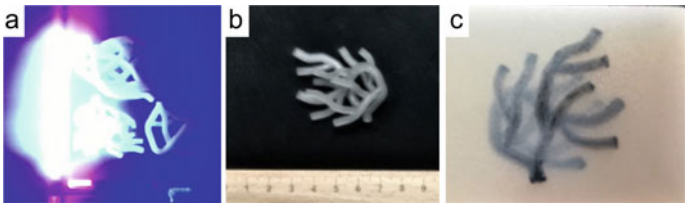

Fig. 4 Phantom manufacturing. **a** 3D printing process. **b** Final model. **c** Final phantom in agar

4.2 Phantoms Realization

Once the 3D model is printed and all wax is removed, the vascular network phantom must be filled with a liquid that can mimic blood, or at the very least absorb and respond to the photoacoustic light impulse. Ideally, real blood or a biocompatible contrast agent should be used. As what is reported here is a proof of concept idea to show the feasibility of the approach, here we simply used a liquid ink that gave forth a strong photoacoustic signal.

The final phantom was then realized using agar, which is a jellying polysaccharide, obtained from red algae and it is used to prepare transparent and neutral gels. Agar powder dissolves at around 90–100 °C and it solidifies at 45 °C. The dose for 1 kg of solution, is 7–10 g of powder.

The desired quantity of agar powder was weighed with a digital scale and then it was put in a small pot with the corresponding quantity of water stirring at the same time. The obtained solution was brought slowly to a boil with a burner continuing to stir and at this point, the warm solution was poured in a container with the vessel model. The phantom was left to cool down and after it solidified, it was pulled out from the container. Figure 4c shows the final phantom filled with dye and inserted in the solidified agar.

4.3 Acquisition Setup

In order to accurately assess vascular complexity, it is clear that a 3D volume of the network must be acquired. It is therefore of fundamental importance to have the phantom model fixed in the same spot and acquire 2D images at a given step size. Some ultrasound systems have a mechanical motor and a corresponding software that permits quick 3D acquisitions at a defined step size. On the other hand, if this is not an option for the system that is used, it is still possible to use a specific setup that guarantees the same position for the ultrasound probe as it runs along the phantom and 2D images are manually acquired at each step.

In our first tests that are presented here, we used the second solution along with a commercial LED-based photoacoustic and ultrasound imaging system (AcousticX, Cyberdyne, INC, Tsukuba, Japan). So, for the image acquisition, the phantoms were fixed to the base of a transparent container filled with water. The ultrasound probe and photoacoustic LED light source arrays were secured to a metallic angle beam, which in turn was fixed to a mobile support that could be moved along a binary in response to a knob rotation. Figure 5 shows the imaging setup used.

The ultrasound probe and LEDs were put underwater near the phantom and linear scans were made moving the system with a defined step size. The step size is what defines the resolution along the third dimension, so a smaller step size would give forth a more accurate volume reconstruction of the vascular network and is fundamental when considering microvasculature.

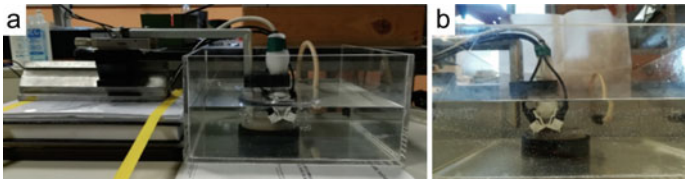

Fig. 5 Imaging setup. **a** Entire imaging setup with metallic angle beam. **b** Zoom on ultrasound probe and LED light sources

Due to the fact that here it was important mainly to show the feasibility of the approach of using 3D LED-based photoacoustic images to evaluate vascular network complexity, and that the phantom vessels had a large diameter compared to microvasculature, we chose to optimize processing time and used a large step size, equal to 1 mm. Considering the model that was designed, this gave forth a final volume that consisted of 65 2D frames.

4.4 Device Settings

The device used for this feasibility study is the AcousticX, a LED-based photoacoustic imaging system (PLED-PAI) that is commercially available [29, 30].

The excitation source are light emitting diodes characterized by high density and high power. Specifically, there are two LED arrays on either side of an ultrasound probe and each array is composed of 4 rows of 36 single embedded LEDs. The excitation wavelength is 850 nm. The dimensions of each array are 12.4 mm (height), 86.5 mm (length) and 10.2 mm (width). The pulse width is variable and can be set from 50 to 150 ns with steps of 5 ns. The pulse repetition rate can be 1, 2, 3 kHz or 4 kHz and it defines consequently the temporal resolution.

In order to reduce noise, it is also possible to control the frame averaging which then influences the frame rate and temporal resolution. The possible frame rates are 30, 15, 10, 6, 3, 1.5, 0.6, 0.3, and 0.15 Hz [7].

For the acoustic part, there is a 128 channels ultrasound linear array transducer with central frequency that can be set between 7 and 10 MHz that can pulse and receive.

For the volume acquisition of the model, only the PA mode was used. The depth was set to 3 cm and the frame rate was 6 Hz. The pulse repetition frequency was set to 4 kHz with 640 frames averaging.

5 Image Processing and Results

After image acquisition, it is then necessary to proceed to segment the images and extract the skeleton of the vascular network in order to compute quantitative vascular parameters that can give an idea of the complexity of the network. In this section of the chapter we will present an example workflow that can be used to extract the quantitative vascular parameters from the acquired images.

5.1 Segmentation and Skeletonization

Before the actual image segmentation, a few preprocessing steps often help in preparing the images and allowing a more accurate segmentation of the objects of interest, which are, in our case, the phantom vessels containing the contrast dye.

Firstly, a 3D median filter was applied to the entire volume, using a $3 \times 3 \times 3$ kernel and padding the volume by repeating border elements in a mirrored way. Then, a closing morphological operation was done using a disk-shaped structuring element with a radius equal to 5 pixels. This step helped fill the vessels where mainly the walls of the phantom were visible.

For the actual segmentation, the Otsu method [31] was used to find the global threshold of each slice and then, the maximum among these was chosen to define a unique threshold for all of the slices of the volume. The images were then segmented using the found threshold, which in our case was equal to 0.43.

Then, a brief cleaning process was used to refine the obtained segmentation. Specifically, each mask was processed by removing all the objects with area smaller than 2% of the biggest object found in the mask. Subsequently, dilatation with a disk-shaped structuring element with radius 3 and erosion with a disk-shaped structuring element with radius 1 were then applied. Finally, any remaining holes in the objects of the mask were then filled. Figure 6 shows a 3D representation of the original photoacoustic images and the obtained segmentation.

For the skeletonization, an algorithm based on the medial axis extraction algorithm by Lee et al. [14] that is implemented preserving the topology and the Euler

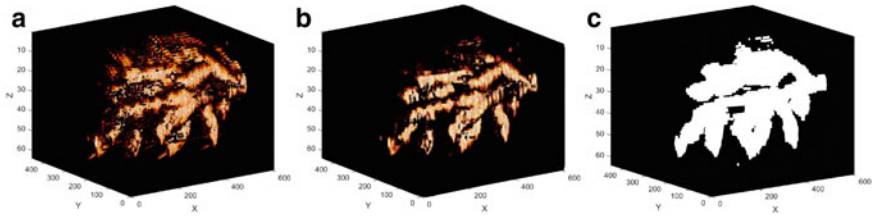

Fig. 6 3D representations. **a** Original photoacoustic image volume. **b** Volume after median filtering. **c** Segmented volume

number was used. This procedure is done to specifically reduce the segmented binary volume into a minimal representation of the vascular network while still preserving morphology.

An algorithm was then implemented with the aim to correct the defects of the skeletonization and to refine the final structure by removing the smallest branches. In some areas of the obtained skeleton, there can be an accumulation of skeleton voxels. In order to remove them, the branchpoints are identified and when, among them, there are connected objects with a value bigger than 10 pixels, they are removed. Thereafter, the branches with a length smaller than a defined threshold are removed.

5.2 Parameter Calculation and Validation

As discussed in a previous section of this chapter, quantitative parameters that give an idea of the morphology and tortuosity of the vascular network can be extracted from the skeleton of the segmented vessels.

In the feasibility study presented here, a 3D computer-aided design (CAD) model was specifically designed and was then printed. This allowed for not only real LED photoacoustic image acquisition once the phantom was correctly filled with a dye, but also the direct importation of the CAD model in the same processing environment (in our case, Matlab).

For validation purposes, the acquired images were also manually segmented so as to give an idea if the automatic segmentation (and therefore the subsequent skeleton) could be considered reliable or not. Then, the recall, precision, and Jaccard index were calculated. These parameters are defined as follows:

$$Recall = \frac{TP}{TP + FN} \tag{1}$$

$$Precision = \frac{TP}{TP + FP} \tag{2}$$

$$JaccardIndex = \frac{TP}{TP + FP + FN} \tag{3}$$

where TP is a true positive, a pixel that was segmented in both the automatic and manual masks; FN is a false negative, a pixel that was segmented only in the manual mask; FP is a false positive, a pixel that was segmented only in the automatic mask.

Furthermore, thanks to the 3D model the quantitative vascular parameters were able to be calculated using the experimental data with the 3D printed phantom and LED photoacoustic image acquisition and also on the imported model using the same skeletonization and vascular parameter computation processes. This type of approach also allows a direct comparison of the quantitative vascular parameters obtained using the various methods. Figure 7 shows different views of the 3D model skeleton together with the automatic skeleton obtained using the acquired images.

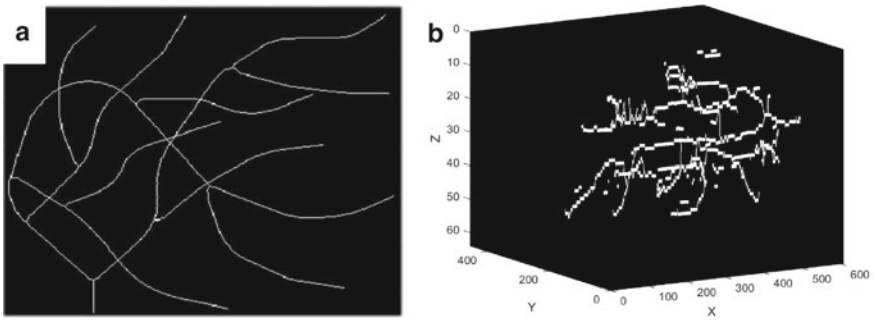

Fig. 7 **a** Top view of skeleton of imported 3D model. **b** 3D skeleton view of automatically segmented volume

6 Feasibility Study Results

Table 1 shows the results of the comparison between the manual and the automatic segmentation of the entire volume of the model. As can be seen, the recall parameter is quite high, showing that when compared to a manual segmentation, the automatic segmentation did not produce many false negatives. This means that the thresholding technique was capable of accurately capturing the photoacoustic signal when it was present within the image. On the other hand, however, the precision is only equal to approximately 72%, meaning that there is a reasonably high number of false positives, so the automatic algorithm was quite sensitive to noise and tended to oversegment the acquired images.

As can be seen in Table 2, the quantitative vascular parameters that were calculated corresponded quite well. In this table, the first column corresponds to the parameters

Table 1 Automatic segmentation validation results

Recall	Precision	Jaccard index
0.94±0.11	0.72±0.18	0.68±0.18

Table 2 Automatic quantitative vascular parameters validation results

Vascular parameter	3D model	Automatic segmentation	Manual segmentation
NT	1	6	6
VD	5.16×10^{-5}	13.69×10^{-5}	15.39×10^{-5}
NB	9	57	77
DM	2.164	2.229	2.289
ICM	67.935	70.197	89.244
SOAM	0.041	0.241	0.545
MR (mm)	0.688±0.174	0.732±0.352	0.591±0.311

computed using the directly imported 3D model, so it can be considered the ground truth. The middle column shows the values computed using the automatic algorithm and segmentation, whereas the last column displays the values obtained when using the manual segmentation.

The biggest discrepancies can be seen within the SOAM tortuosity parameter and the number of trees and number of branch nodes of the vascular network. It is important to point out here how not only the automatic segmentation but also the manual segmentation provided an overestimation of these parameters. This is most likely due to the fact that, during the phantom manufacturing process, it was seen that some parts of the phantom were not properly filled with the ink due to the presence of remaining wax, resulting in no or less photoacoustic signals from those points. At the same time, it is also important to underline how the 3D model was imported into MATLAB with a very good spatial resolution, providing a perfectly clean and rounded vessel mask. So, the acquired images were limited by a number of various issues. Specifically, the obtained results were limited by (a) the high step size and therefore low resolution between slices, (b) any small air bubble or imperfect filling of the model with the dye, and (c) photoacoustic imaging artefacts which are common especially when employing linear ultrasound probes for the photoacoustic signal reception.

7 Conclusion

While the feasibility study presented here showed some limitations, mainly due to phantom manufacturing and an imperfect wax removal technique, the results are promising and merit a further investigation using even more complex vascular phantoms at first and then using in vivo images considering micro-vasculature to evaluate the resolution limits of this approach. Overall, the proof of concept study shown here in this chapter demonstrates the potential of evaluating vascular complexity using 3D LED-based photoacoustic images.

References

1. E. Bullitt, K.E. Muller, I. Jung, W. Lin, S. Aylward, Analyzing attributes of vessel populations. Med. Image Anal. **9**(1), 39–49 (2005)
2. E. Bullitt, S.R. Aylward, T. Van Dyke, W. Lin, Computer-assisted measurement of vessel shape from 3T magnetic resonance angiography of mouse brain. Methods **43**(1), 29–34 (2007)
3. S.E. Shelton et al., Quantification of microvascular tortuosity during tumor evolution using acoustic angiography. Ultrasound Med. Biol. **41**(7), 1896–1904 (2015)
4. K.M. Meiburger, S.Y. Nam, E. Chung, L.J. Suggs, S.Y. Emelianov, F. Molinari, Skeletonization algorithm-based blood vessel quantification using in vivo 3D photoacoustic imaging. Phys. Med. Biol. **61**(22) (2016)
5. J.T. Perry, J.D. Statler, Advances in vascular imaging. Surg. Clin. North Am. **87(**5), 975–993 (2007)

6. Y. Zhang, H. Hong, W. Cai, *Photoacoustic Imaging* (Spring, Berlin, 2011)
7. A. Hariri, J. Lemaster, J. Wang, A.K.S. Jeevarathinam, D.L. Chao, J.V. Jokerst, The characterization of an economic and portable LED-based photoacoustic imaging system to facilitate molecular imaging. Photoacoustics **9**, 10–20 (2018)
8. P. Beard, Biomedical photoacoustic imaging. Interface Focus **1**(4), 602–631 (2011)
9. E.Z. Zhang, J.G. Laufer, R.B. Pedley, P.C. Beard, In vivo high-resolution 3D photoacoustic imaging of superficial vascular anatomy. Phys. Med. Biol. **54**(4), 1035–1046 (2009)
10. B. Preim, S. Oeltze, 3D visualization of vasculature: an overview (2008), pp. 39–59
11. S. Moccia, E. De Momi, S. El Hadji, L. S. Mattos, Blood vessel segmentation algorithms—review of methods, datasets and evaluation metrics. Comput. Methods Programs Biomed. **158**, 71–91 (2018) Elsevier Ireland Ltd
12. C. Kirbas, F.K.H. Quek, Vessel extraction techniques and algorithms : a survey, in *Proceedings—3rd IEEE Symposium on BioInformatics and BioEngineering, BIBE 2003*, (2003), pp. 238–245
13. A.F. Frangi, W.J. Niessen, K.L. Vincken, M.A. Viergever, Multiscale vessel enhancement filtering, in *International Conference on Medical Image Computing and Computer-Assisted Intervention*, (1998), pp. 130–137
14. T.C. Lee, R.L. Kashyap, C.N. Chu, Building skeleton models via 3-D medial surface axis thinning algorithms. CVGIP Graph. Model. Image Process. **56**(6), 462–478 (1994)
15. T. Chan, L. Vese, Active contours without edges. IEEE Trans. Image Process. **10**(2), 266–277 (2001)
16. Y.S. Zhang, J. Yao, C. Zhang, L. Li, L.V. Wang, Y. Xia, Optical-resolution photoacoustic microscopy for volumetric and spectral analysis of histological and immunochemical samples. Angew. Chem. Int. Ed. Engl. **53**(31), 8099–8103 (2014)
17. Z. Yang et al., Multi-parametric quantitative microvascular imaging with optical-resolution photoacoustic microscopy in vivo. Opt. Express **22**(2), 1500–1511 (2014)
18. T. Tozaki, Y. Kawata, N. Niki, H. Ohmatsu, N. Moriyama, 3-D visualization of blood vessels and tumor using thin slice CT images, in *IEEE Nuclear Science Symposium and Medical Imaging Conference*, vol. 3, (1995), pp. 1470–1474
19. U.R. Acharya, O. Faust, S.V. Sree, F. Molinari, J.S. Suri, ThyroScreen system: high resolution ultrasound thyroid image characterization into benign and malignant classes using novel combination of texture and discrete wavelet transform. Comput. Methods Programs Biomed. **107**(2), 233–241 (2012)
20. F. Molinari, A. Mantovani, M. Deandrea, P. Limone, R. Garberoglio, J.S. Suri, Characterization of single thyroid nodules by contrast-enhanced 3-D ultrasound. Ultrasound Med. Biol. **36**(10), 1616–1625 (2010)
21. F. Molinari et al., Quantitative assessment of cancer vascular architecture by skeletonization of high-resolution 3-D contrast-enhanced ultrasound images: role of liposomes and microbubbles. Technol. Cancer Res. Treat. **13**(6), 541–550 (2014)
22. K.M. Meiburger et al., Automatic skin lesion area determination of basal cell carcinoma using optical coherence tomography angiography and a skeletonization approach : Preliminary results. J. Biophotonics, no. April, 1–11 (2019)
23. E. Bullitt, G. Gerig, S.M. Pizer, W. Lin, S.R. Aylward, Measuring tortuosity of the intracerebral vasculature from MRA images. IEEE Trans. Med. Imaging **22**(9), 1163–1171 (2008)
24. W.C. Vogt, C. Jia, K.A. Wear, B.S. Garra, T.J. Pfefer, Biologically relevant photoacoustic imaging phantoms with tunable optical and acoustic properties. J. Biomed. Opt. **21**(10), 101405 (2016)
25. M. Fonseca, B. Zeqiri, P. Beard, B. Cox, Characterisation of a PVCP based tissue-mimicking phantom for Quantitative Photoacoustic Imaging, in *Opto-Acoustic Methods and Applications in Biophotonics II*, (2015), p. 953911
26. S.E. Bohndiek, S. Bodapati, D. Van De Sompel, S.-R. Kothapalli, S.S. Gambhir, Development and application of stable phantoms for the evaluation of photoacoustic imaging instruments. PLoS ONE **8**(9), e75533 (2013)

27. J.R. Cook, R.R. Bouchard, S.Y. Emelianov, Tissue-mimicking phantoms for photoacoustic and ultrasonic imaging. Biomed. Opt. Express **2**(11), 3193 (2011)
28. Y. Guo, H.S. Patanwala, B. Bognet, A.W.K. Ma, Inkjet and inkjet-based 3D printing: Connecting fluid properties and printing performance. Rapid Prototyp. J. **23**(3), 562–576 (2017)
29. N. Sato, M. Kuniyil Ajith Singh, Y. Shigeta, T. Hanaoka, T. Agano, High-speed photoacoustic imaging using an LED-based photoacoustic imaging system, in *Photons Plus Ultrasound: Imaging and Sensing 2018*, (2018), p. 128
30. J. Joseph et al., Characterization and technical validation of a multi-wavelength LED-based photoacoustic/ultrasound imaging system (Conference Presentation), in *Photons Plus Ultrasound: Imaging and Sensing 2018*, 2018, p. 34
31. N. Otsu, A threshold selection method from gray-level histograms. IEEE Trans. Syst. Man. Cybern. **9**(1), 62–66 (1979)